LETTER • OPEN ACCESS

Intensification of the East Asian summer monsoon lifecycle based on observation and CMIP6

IOP Publishing Environ. Res. Lett. 15 (2020) 0940b9 https://doi.org/10.1088/1748-9326/ab9b3f

Environmental Research Letters

OPEN ACCESS

RECEIVED
31 December 2019

REVISED
28 May 2020

ACCEPTED FOR PUBLICATION
10 June 2020

PUBLISHED
11 September 2020

LETTER

Intensification of the East Asian summer monsoon lifecycle based on observation and CMIP6

Jina Park[1], Hyungjun Kim[2], S -Y Simon Wang[3], Jee-Hoon Jeong[4], Kyo-Sun Lim[5], Matthew LaPlante[3,6] and Jin-Ho Yoon[1,7]

[1] School of Earth Sciences and Environmental Engineering, Gwangju Institute of Science and Technology, Gwangju, Korea
[2] Institute of Industrial Science, The University of Tokyo, Tokyo, Japan
[3] Department of Plants, Soils, and Climate, Utah State University, Logan, UT, United States of America
[4] Department of Oceanography, Chonnam National University, Gwangju, South Korea
[5] School of Earth System Sciences, Kyungpook National University, Daegu, South Korea
[6] Department of Journalism and Communication, Utah State University, Logan, UT, United States of America
[7] Author to whom any correspondence should be addressed.

E-mail: yjinho@gist.ac.kr

Keywords: East Asian summer monsoon, extreme, flood, drought

Abstract

Long-term changes in the East Asian summer monsoon (EASM) lifecycle since 1979 are analyzed based on observational datasets and historical simulations of the Coupled Model Intercomparison Project Phase 6 (CMIP6). According to the observation, the active and break phases of EASM have intensified resulting in a shorter but stronger rainy season, followed by a longer dry spell. This intensification in the active-phase precipitation is accompanied by increased lower tropospheric southwesterly wind and subsequent convergence of water vapor flux. These changes are accompanied by the widely reported westward extension of the North Pacific Subtropical High, which has been associated with the warming climate. CMIP6 models generally underestimated the observed intensification of the EASM lifecycle and the monsoon precipitation. However, some of the models did simulate the intensified EASM lifecycle similar to that observed. The result highlights the reasonable performance on EASM shown in some CMIP6 models and those simulations lend support to a dynamically-driven intensification of the EASM lifecycle in the warmer climate.

1. Introduction

Throughout East Asia, summer precipitation variability in intraseasonal timescales has been increasing, resulting in more frequent floods and intense dry spells seemingly coexisted during the same season. Summer rainfall in northeast Asia is driven by the distinct lifecycle of the East Asian Summer Monsoon (EASM). The EASM lifecycle includes a stepwise northward and northeastward advance, derived from successive passages through (i) its rainbands (Changma, Meiyu, or Baiu), (ii) the western Pacific subtropical high, and (iii) tropical cyclone activity (Chen *et al* 2004, Yihui and Chan 2005). As a result, the EASM features active, break, and revival phases, with intraseasonal timing of these phases dependent upon location. The intensification of this lifecycle was manifest in the 2018 Japan flood-heat wave succession event, in which more than 1000 people were killed in one month (Imada *et al* 2019, Wang *et al* 2019).

The temporal and spatial variability associated with the EASM lifecycle makes trend analysis difficult and produces geographically inconsistent results. Several studies have indicated that summer precipitation over East Asia has increased (Kim *et al* 2005, In *et al* 2014, Kornhuber *et al* 2019), but rainfall trends also vary by month. In Korea, Kim *et al* (2005) found an overall increase in summer precipitation, while In *et al* (2014) found that only July and August saw increased precipitation.

The impact of global warming on the EASM is an ongoing dispute. Several studies have asserted that global warming has increased EASM precipitation (Yun *et al* 2008, Seo *et al* 2013, Wang *et al* 2018, Jin and Stan 2019, Madakumbura *et al* 2019), but opposite trends regarding EASM precipitation have also been reported (Zhu *et al* 2012, Burke and Stott 2017).

Table 1. Observational dataset description.

Variable	Dataset	Horizontal resolution	Analysis period	Reference
Precip-itation	Unified CPC	0.5°× 0.5°	1979–2017	Xie *et al* (2007)
	APHRODITE	0.25°× 0.25°	1979–2015	Yatagai *et al* (2012)
	GPCP 1DD	1.0°× 1.0°	1997–2015	Huffman *et al* (2001)
OLR	NCEI	2.5°× 2.5°	1979–2017	Liebmann and Smith (1996)
Meteorolo-gical variable	JRA-55	1.25°× 1.25°	1979–2017	Harada *et al* (2016); Kobayashi *et al* (2015)
	ERA-interim	0.75°× 0.75°	1979–2017	Dee *et al* (2011)

These seemingly conflicting claims arguably result from the limitation of climate models in simulating EASM features (Liu *et al* 2018, Tian *et al* 2019). Additionally, the coexistence of various weather systems in East Asia (Utsumi *et al* 2017) and their nonlinear changes with global warming have further complicated the matter (Utsumi *et al* 2016). Meanwhile, Li *et al* (2010) have suggested the chance of both drought and flood over East Asia would increase together due to global warming, a proposition that may reconcile these notions.

In this paper, we analyzed the variability of the EASM lifecycle and subsequently evaluated the performance of coupled climate models in CMIP6. In section 2, we described the observational and modeling datasets as well as the analysis methods. Section 3 shows the observed intensification to the EASM lifecycle and the variability in the CMIP6 models. A conclusion is provided in section 4.

2. Data and method

2.1. Data

Daily precipitation data is obtained from the Climate Prediction Center Global Unified Precipitation dataset provided by the NOAA Earth System Research Laboratory's Physical Sciences Division at https://www.esrl.noaa.gov/psd/. Spatial coverage is the global terrestrial area on a half degree grid. Daily outgoing longwave radiation (OLR), daily precipitation data from Asian Precipitation Highly Resolved Observational Data Integration Towards Evaluation (APHRODITE), and from GPCP Version 1.2 are used to check the robustness of the change in unified CPC (table 1). Global 6-hourly meteorological data (850mb geopotential height, u-wind, and v-wind, and column integral of horizontal water vapor flux) at the 1.25°× 1.25° resolution is obtained from JRA-55 (Kobayashi *et al* 2015, Harada *et al* 2016). We also used the ERA-interim dataset for comparison (Dee *et al* 2011).

To assess the CMIP6 model performance, we adopted a single ensemble member from the historical simulations of 32 different models retrieved from the PCMDI database; these models are summarized in table 2. Following the sampling approach of Knutti *et al* (2010), only one member from each model experiment was selected to avoid potential systematic bias when calculating linear trends from the multi-model ensemble mean. CMIP6 outputs are linearly interpolated to 0.5 × 0.5°, same as the unified CPC rainfall dataset and ocean masking is applied. The analysis period is from 1979 to 2010 for the CMIP6 historical runs and from 1979 to 2017 for the reanalysis data. In case of precipitation from APHRODITE and GPCP, the analysis period is from 1979 to 2015 and from 1997 to 2015 respectively, due to data accessibility.

2.2. Methods

This study categorizes East Asia into three subregions, including the Korean peninsula (125°-130°E, 33°-38°N), the central-eastern part of China (115°-120°E, 27°-33°N), and the south-western part of Japan (130°-139°E, 31°-38°N) as shown in figure 1 inset. The EASM lifecycle has three-phases (active, break, and revival) but the variability of revival is mixed with tropical cyclone activity. Thus, this study focuses on active and break phases only. Various meteorological variables have been used to define the onset and withdrawal of the monsoon rainband (Ellis *et al* 2004, Yihui and Chan 2005, Seo *et al* 2011, Pradhan *et al* 2017); however, for simplicity, we used daily climatology of precipitation to define the active and break phases.

Researchers have previously defined the Changma onset as the first day of more than 3 d of at least 5 mm d^{-1} rainfall (Seo *et al* 2011), but a defined active period based on this criteria is not always aligned with the operational active period. For example, the active period in Korea under this criteria is defined from 17 June to 5 September, but operationally the Korean Meteorological Agency defined the active phase from 19 June to 24 July (Seo *et al* 2011) and the Japan Meteorological Agency defined the active phase in Kyushu from 5 June to 19 July. [1] Here, the active phase is defined by 3 consecutive days of rainfall greater than 6 mm d^{-1} and the break phase is defined as the 14 d after the active phase. Figures 1(a)–(c) display the rainfall pattern and timing of the active phase and subsequent break over Korea, central-eastern China, and southwestern Japan. The dates for active, peak and break phases are listed in table 3, which is comparable to those used in the regional operational centers.

[1]Japan Meteorological Agency provide information about meiyu rainband from web site at http://www.data.jma.go.jp/.

Table 2. CMIP6 model description.

Model	Country and institute	Resolution
ACCESS-CM2	Australia, CSIRO-ARCCSS	192 * 144
ACCESS-ESM1-5	Australia, CSIRO-ARCCSS	192 * 145
BCC-CSM2-MR	China, BCC	320 * 160
BCC-ESM1	China, BCC	128 * 64
CESM2	USA, NCAR	288 * 192
CESM2-FV2	USA, NCAR	144 * 96
CESM2-WACCM	USA, NCAR	288 * 192
CESM2-WACCM-FV2	USA, NCAR	144 * 96
CNRM-CM6-1	France, CNRM-CERFACS	256 * 128
CNRM-CM6-1-HR	France, CNRM-CERFACS	720 * 360
CNRM-ESM2-1	France, CNRM-CERFACS	256 * 128
CanESM5	Canada, CCCma	128 * 64
EC-Earth3	Europe, EC-Earth-Consortium	512 * 256
EC-Earth3-Veg	Europe, EC-Earth-Consortium	512 * 256
FGOALS-f3-L	China, CAS	288 *180
FGOALS-g3	China, CAS	180 * 80
GFDL-CM4	USA, NOAA	288 * 180
GFEL-ESM4	USA, NOAA	288 * 180
INM-CM4-8	Russia, INM	180 * 120
INM-CM5-0	Russia, INM	180 * 120
IPSL-CM6A-LR	France, IPSL	144 * 143
MIROC-ES2L	Japan, MIROC	128 * 64
MIROC6	Japan, MIROC	256 * 128
MPI-ESM-1-2-HAM	Germany, MPI-M	192 * 96
MPI-ESM1-2-HR	Germany, MPI-M	384 * 192
MPI-ESM1-2-LR	Germany, MPI-M	192 * 96
MRI-ESM2-0	Japan, MRI	320 * 160
NESM3	China, NUIST	192 * 96
NorCPM1	Norway, NCC	144 * 96
NorESM2-LM	Norway, NCC	144 * 96
NorESM2-MM	Norway, NCC	288 * 192
TaiESM1	Taipei, AS-RCEC	288 * 192

In order to examine the extreme precipitation, 'peak phase' is defined as the days in which rainfall exceeds 8 mm d^{-1} over 1 standard deviation in all three regions. To estimate the dry spell associated with the break phase, we have introduced the Dry Severity Index (DSI), which is defined as the product of the dry spell length and precipitation deficit. Dry spell length (DSL) reflects the duration of the dry event and is the length of the successive dry days (P = 0). Precipitation deficit (PD) reflects the magnitude of a dry event (Tallaksen *et al* 1997) and is defined as three times the long-term mean precipitation for break periods over time ($\bar{P}$) minus annual precipitation ($P(t)$) divided by mean precipitation. (Multiplying the long-term mean precipitation by three ensures PD is always positive and thus simplifies the interpretation.)

$$DSI = DSL \times PD \tag{1}$$

$$PD = \frac{(3 \times \bar{P} - P(t))}{\bar{P}}. \tag{2}$$

In the atmosphere, the amount of water vapor (E–P) is the sum of the water vapor mass change depending on time and water vapor flux transfer (Barnes 1965) (equation (3)). The sum of the water vapor changes ($\frac{\partial w}{\partial t}$) is small and negligible. At the surface, the convergence of water vapor flux ($-\nabla \cdot Q$) infers the amount of moisture pooling (equation (4)).

$$\frac{\partial w}{\partial t} + \nabla \cdot Q = E - P \tag{3}$$

$$where, w = \frac{1}{g}\int qdP,\ Q = \int \vec{v}qdP,\ P\ is\ precipitation,\ E\ is\ evaporation$$

$$P - E = -\nabla \cdot Q. \tag{4}$$

3. Results

3.1. Observational analysis

Linear trends of rainfall in the active and break phases were examined in figure 2 for the three target regions. During the active phase, positive precipitation trends prevail in most areas (figure 2(a)). Active phase precipitation over East Asia has increased (figure 2(c)) and the trend is more pronounced in the peak rainfall of the active phase (figure 2(e)). In Japan, a strong positive trend in the southwest (Kyushu)

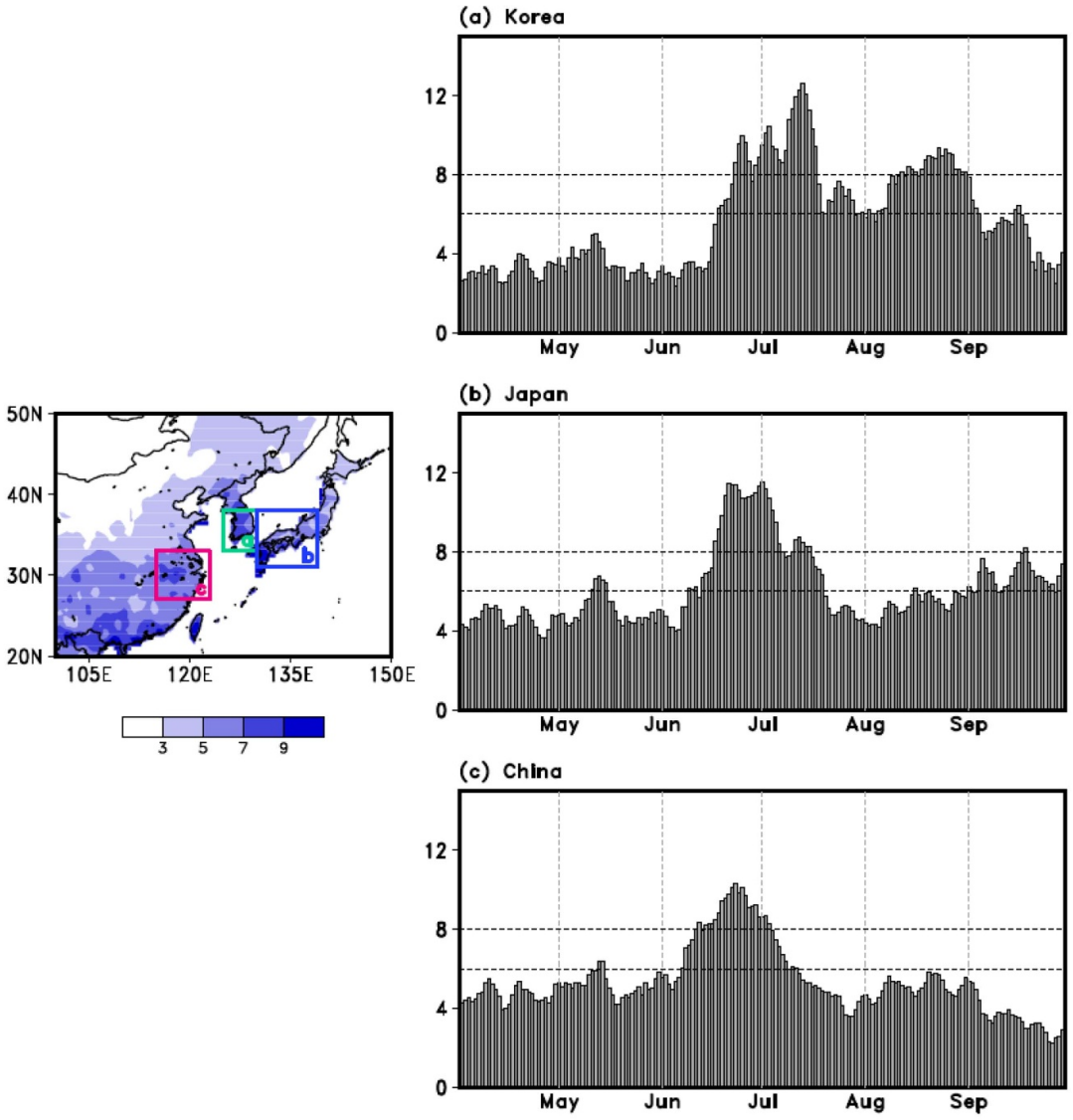

Figure 1. Left: mean precipitation [mm day^{-1}] during JJA (Jun-July-August) from unified CPC. Right: five day running mean of daily climatology based on unified CPC over three target regions: (a) Korea, (b) Japan, and (c) China, marked as green, blue, red boxes on the left figure. Dotted line at the 6mm day^{-1} and 8mm day^{-1} indicates the threshold for active and peak phase, respectively.

dominates weak negative trends in the Osaka and Nagoya regions. For both active and peak phases, the precipitation trend over Japan is consistently significant ($p<0.05$) but in Korea, the increasing trend is only significant in the peak in active phase ($p<0.1$). This contrasts with precipitation trend over China, which is only significant in the active phase ($p<0.1$) but not in its peak phase. Nonetheless, the active phase precipitation has increased and this observation suggests enhanced EASM rainfall in active over time. This result is in agreement with a recent study on Taiwan's EASM active rainfall (Tung *et al* 2020).

During the monsoon break phase, figure 2(b) shows a negative trend in precipitation in Korea and central-eastern China, while a weak but positive trend is exhibited in southwest Japan. In terms of the break phases over each region, the linear trend is weak and statistically insignificant (figure 2(d)). To examine the reduced precipitation amount during the break phase, we calculated the dry severity index (DSI) described above to examine the intensity and duration of precipitation reduction together (figure S1 (available online at stacks.iop.org/ERL/15/0940b9/mmedia)). Although the trend is not statistically significant, dry spells have become drier and have lasted longer, with the exception of central-eastern China. The severity of dry periods in Korea and southwest Japan has increased. Combined, these findings indicate that the overall EASM lifecycle has enhanced, leading to a higher chance of both wet and dry extremes within a single summer season. This is consistent with the results of Singh *et al* (2014) and Li *et al* (2010) for the long-term trends, as well as the consecutive flood-heat wave events over Japan during the summer of 2018 (Wang *et al* 2019).

Table 3. The dates for the active and break phases for each region in our study domain.

	Korea	Japan	China
Active	18 Jun–18 Jul	13 Jun–19 Jul	07 Jun–11 Jul
Peak	29 Jun–17 Jul	17 Jun–07 Jul	11 Jun–04 Jul
Break	19 Jul–01 Aug	20 Jul–02 Aug	12 Jul–25 Jul

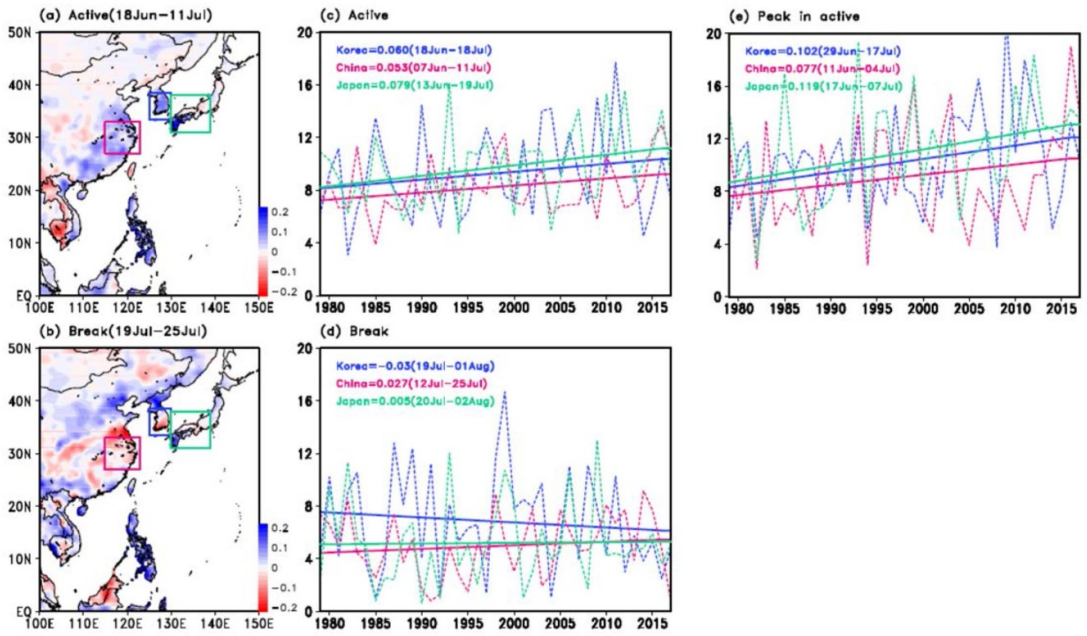

Figure 2. Linear trend of precipitation [mm day^{-1} yr^{-1}] for (a) overlapped active period among three regions (18Jun – 11Jul), (b) overlapped break period among three regions (19Jul – 25Jul), and linear trend of precipitation in (c) active, (d) break, and (e) peak in active. Data is from unified CPC and each period in (c), (d), and (e) is referred from Table 3.

Temporal and latitudinal evolution of rainfall is investigated using a latitude-time Hovmöller diagram (figure 3(a)). Climatologically, the rainband propagates northward and passes East Asia from early June to mid-July. As the rainband passes East Asia, it causes the Meiyu-Baiu-Changma season from central eastern China to southwest Japan to Korea, respectively, with increased precipitation observed along this migrating rainband in the Meiyu stage (~25°N). A slight drying trend is observed in the periods before and after this rainband passage, suggesting the EASM rainband has intensified and this intensification is associated with adjunct drying. There is dry signal over East Asia from mid-July, proposing enhanced dry signal in break phase. The result is robust regardless of the other datasets used (see figure S2 for the validation analysis). ΔOLR, which is defined as 235-OLR, values larger than zero is used in this analysis as an indicator of deep convection. The trend of precipitation from GPCP is not calculated because the analysis period is too short. APHRODITE, GPCP, and OLR all show consistent result with that from the unified CPC precipitation. Since the characteristics of each precipitation data are unique, their consistent trends lend support to the robustness of the life-cycle change of the EASM precipitation.

The rainfall migration in summer over East Asia is closely related with the low-level southwesterlies (Seo *et al* 2013), so we defined the temporal evolution of the 850 hPa south westerlies as $SW = u * \sin(45°) + v * \cos(45°)$ and the convergence of water vapor. As shown in the Hovmöller diagram (figures 3(b)), the rainband's evolution coincides with that of the southwesterly wind and their trends are in phase, suggesting that the increased precipitation along the EASM rainband may be dynamically driven. Next, we plotted the migration of convergence of water vapor in figure 3(c) and found that the migrating pattern of $-\nabla \cdot Q$ agrees well with that of the precipitation and southwesterly wind, both in the climatology and the respective trends. Noteworthy is the similar but opposite trends in $-\nabla \cdot Q$ suggesting that the drying trends adjacent to the EASM rainband are accompanied by increased divergence of water vapor flux. The climatology and trend of the south westerlies and $-\nabla \cdot Q$ were crosschecked with the ERA-interim dataset (figure S3), and the result is robust regardless of which dataset used. The cause of these systematic changes may be related to the documented westward expansion of the Western North Pacific Subtropical High (WNPSH) in the warmer world. As shown in figure S4, the WNPSH

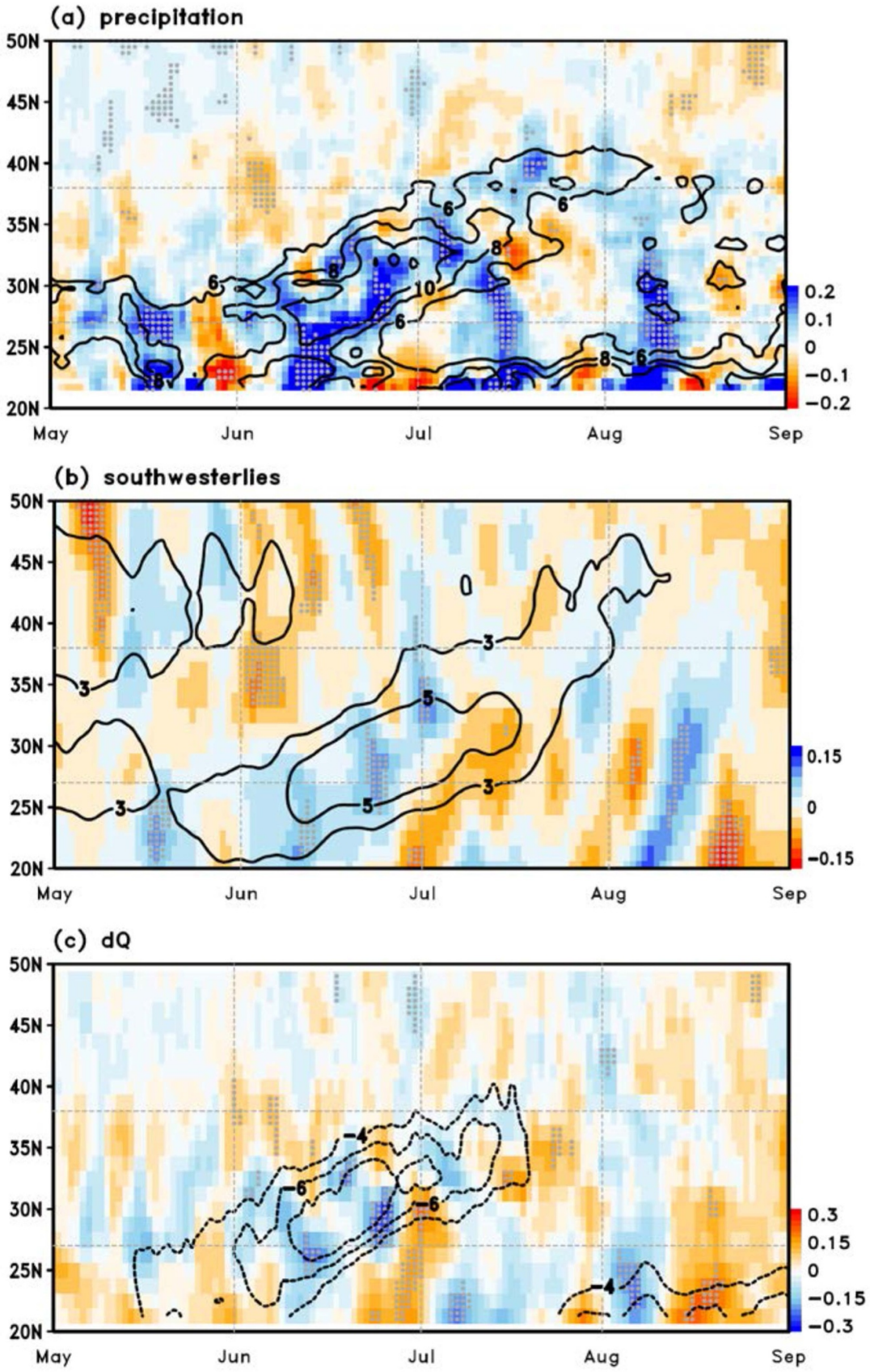

Figure 3. Hovmöller diagram for time (x) – latitude (y) of five day running mean of (a) rainfall [mm day^{-1}] from unified CPC, (b) 850mb southwesterlies [m s^{-1}] from JRA-55, and (c) divergence of Q [10^{-5} kg m^{-1} s^{-1}] from JRA-55 and averaged from 115E to 139E covering target area. Contour is climatology and distinct value is plotted. (a. 6 ~ 10mm day^{-1}; b. 3 ~ 5m s^{-1}; c. -8 ~ -4 *10^{-5} kg m^{-1} s^{-1}). The trend is shaded ranging (a) from -0.2mm day^{-1} yr^{-1} to 0.2mm day^{-1} yr^{-1}, (b) from -0.15m s^{-1} yr^{-1} to 0.15m s^{-1} yr^{-1} and (c) -0.3*10^{-5} kg m^{-1} s^{-1} yr^{-1} to 0.3*10^{-5} kg m^{-1} s^{-1} yr^{-1}, respectively. Dotted area is significant at 95% confidence level.

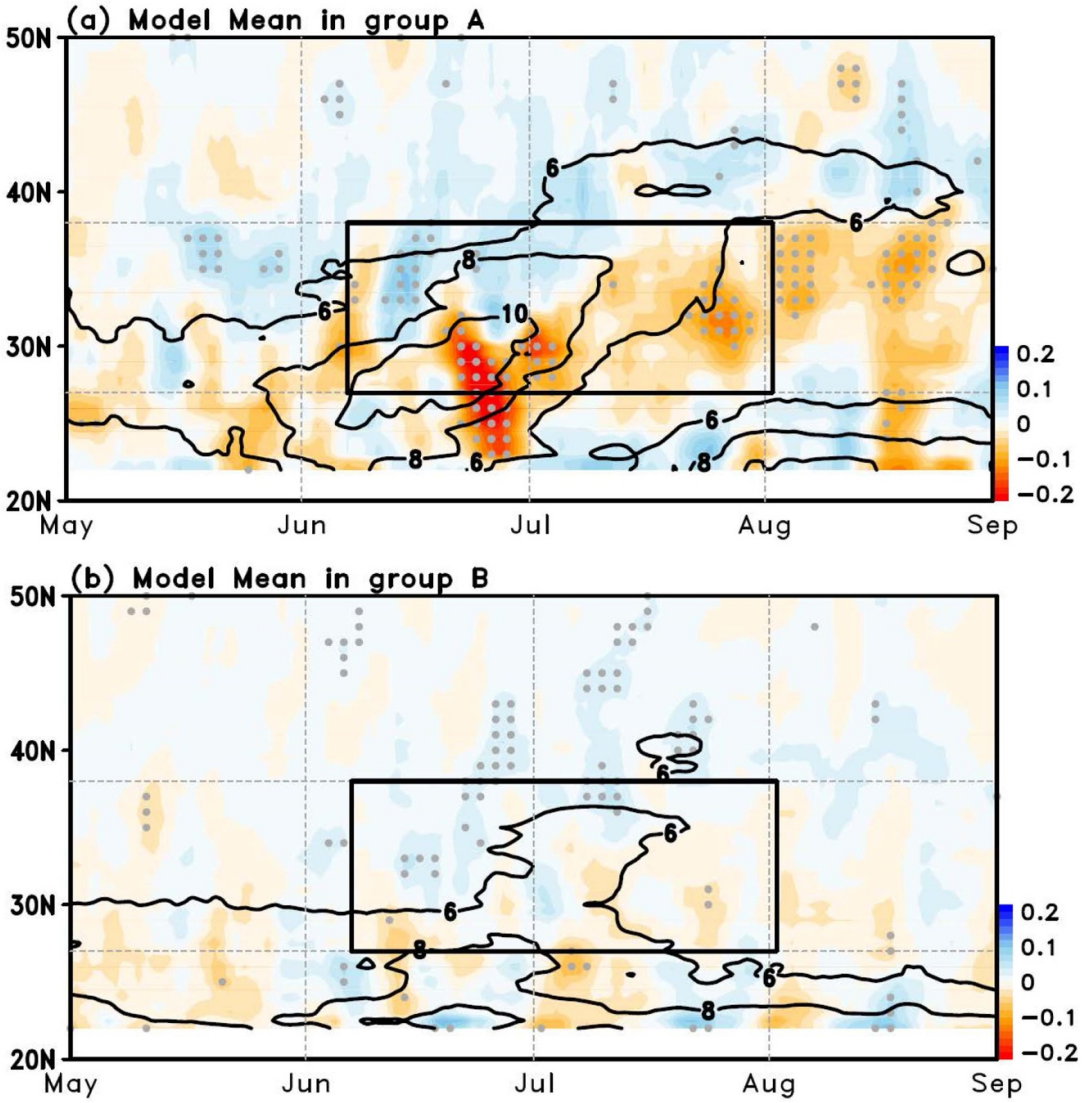

Figure 4. Hovmöller diagram for time (x) – latitude (y) same as Figure 3(a), but those from multi-model ensemble mean of models in group (a) A and (b) B in CMIP6.

has expanded westward in recent decades causing the high pressure to arrive earlier and reach farther in East Asia, hence increasing the south-westerlies. This finding echoes the observation by Woo *et al* (2017) that the Changma rainfall has increased due to the expansion of WNPSH modulating the jet-stream over Korea and inducing anomalous anti-cyclones south of Korea. Intensified southerly and southwesterly winds also cause moist convection to increase, eventually enhancing the EASM precipitation (Seo *et al* 2013).

3.2. Simulation by CMIP6 models

Next, we examined the historical simulations of CMIP6 for evaluation. The similarity of the observations and the simulated climatological features of EASM lifecycle is quantitatively evaluated using the pattern correlation that is illustrated on a Hovmöller diagram of precipitation (here, *x*- and *y*-axis are for time and latitude, respectively) of precipitation. For active and break phases over East Asia (latitude of 27°N-38°N, and time period from 7 June to 2 August in figure 4), the pattern correlation between observations and CMIP6 models was calculated to examine how the models catch the migrating pattern. However, it does not consider the intensity of the precipitation, so we included that averaged precipitation amount as an additional measure. CMIP6 models with R^2 larger than 0.5 and the total averaged precipitation for active and break phases over East Asia within ± 20% of observations (7.54) are categorized as 'group A' and the others as 'group B'. In the end, 8 models and 24 models are in group A and B, respectively (table 4). Interestingly, strong correlation between climatological rainfall and its long-term change measured by pattern correlation (figure S5) strongly infers importance of better climatological rainfall in the EASM.

Table 4. Pattern correlation coefficient in CMIP6 model. Correlation coefficient larger than 0.70 ($r^2 > 0.5$) and total precipitation for active and break phase over East Asia is within ± 20% of observation (6.03–9.05) is classified as group A, and the others are in group B.

	Model	Corr. Coeff.	Total Precipitation
Group A	CESM2	0.76	8.32
	CESM2-FV2	0.74	7.80
	CESM2-WACCM	0.86	8.25
	CESM2-WACCM-FV2	0.73	7.37
	INM-CM5-0	0.71	7.84
	NorESM2-LM	0.75	7.51
	NorESM2-MM	0.86	7.58
	TaiESM1	0.86	8.02
Group B	ACCESS-CM2	0.29	5.19
	ACCESS-ESM1-5	−0.12	3.96
	BCC-CSM2-MR	0.63	5.35
	BCC-ESM1	0.63	5.40
	CanESM5	0.31	5.22
	CNRM-CM6-1	0.28	5.99
	CNRM-CM6-1-HR	0.50	6.51
	CNRM-ESM2-1	0.46	6.05
	EC-Earth3	0.45	5.58
	EC-Earth3-Veg	0.58	5.64
	FGOALS-f3-L	0.32	5.70
	FGOALS-g3	0.61	5.58
	GFDL-CM4	0.28	5.08
	GFDL-ESM4	0.20	4.65
	INM-CM4-8	0.55	7.86
	IPSL-CM6A-LR	0.58	6.28
	MIROC-ES2L	0.49	6.76
	MIROC6	0.45	6.32
	MPI-ESM-1-2-HAM	0.50	5.53
	MPI-ESM1-2-HR	0.53	6.37
	MPI-ESM1-2-LR	0.47	5.52
	MRI-ESM2-0	0.29	4.94
	NESM3	0.42	5.33
	NorCPM1	0.60	6.37

The climatology of the spatiotemporal evolution of precipitation (solid line) is reasonably simulated (figure 4), though simulated precipitation in models both in group A and B tends to be underestimated. Models in group A depict the climatological rainfall onset and its migration to the north well (figure 4(a)). However, the intensity of precipitation is weak. There is a slightly positive trend at the beginning of the rainband, but a negative trend exists throughout the monsoon period, implying underestimation of the EASM precipitation. Precipitation time-series for the overlapping active, break and peak phases in three regions are shown in figure S6. Observations show a distinct increasing trend in the active and peak phases and decreasing trend in break phase, supporting the observed intensification of the EASM lifecycle. Precipitation of group A models shows a distinct decreasing trend in the break phase and slightly increasing trend in active and peak phases. Despite the underestimated precipitation in group A models, northward propagation of the rainband, intraseasonal characteristic, is realistically simulated. Furthermore, the overall pattern of wetting trend (drying trend) in the earlier (later) part of the rainy season is well simulated. All models in group A do simulate climatological propagation of the rainband but the timing and the intensity of the monsoon onset are different (figure S7). Nevertheless, some models in group A (CESM2, CESM2-WACCM, CESM2-WACCM-FV2) reproduce the intensification in both the active and break phases (figure S9). When it comes to models in group B, the rainfall peak in summer is captured but the amount of precipitation is underestimated and they mostly fail to simulate the migrating pattern of EASM (figure 4(b)). Nevertheless, some models depict the climatological propagation of the rainband, but the rainband reaches to the East Asia lately or its intensity is weak (CNRM-CM6-1, CNRM-CM6-1-HR, CNRM-ESM2-1, EC-Earth3, EC-Earth3-Veg, INM-CM4-8, IPSL-CM6A-LR, MIROC-ES2L, MIROC6, NorCPM1) (figure S8). Also, most models fail to simulate the precipitation trend in either phase except for EC-Earth3, MIROC6, CNRM-CM6-1 (figure S8). These models catch the wetting trend (drying trend) in the earlier (later) part of the rainy season, but the timing of the rainy season is wrong. The climatological propagation of the rainband simulated by EC-Earth3 and MIROC6 is too fast and the rainband reproduced by CNRM-CM6-1 is stagnated at the lower latitude. Time-series of

precipitation for overlapped active, break, and peak of MIROC6 phases show similar trend with that of observation (figure S10).

According to previous studies of Park *et al* (2020) and Li *et al* (2020) using CMIP5 models, it was found that certain features of the EASM were simulated but its more detailed characteristics were not properly captured, such as the second peak and northward propagation of precipitation. On the other hand, some of CMIP6 models, those in group A simulate the EASM lifecycles and its long-term change, which is a positive sign.

4. Concluding remarks

In this paper, the long-term change in the EASM lifecycle was analyzed based on observational datasets, and the capacity of CMIP6 models to reproduce the mechanisms of the long-term trends. It was found that precipitation in the active phase has increased and the increasing trend is more significant in its peak, which means that the monsoon peak or extremes is getting stronger. This precipitation trend coincides with the increasing trends of southwesterly wind and the convergence of water vapor flux accompanying the rainband. The WNPSH and its westward extension help intensify the southwesterly wind. It was also found that the break phase tends to be enhanced after the rainband passage, and this tendency is further illustrated by the DSI index, showing the combined intensity and duration of the dry spell. Thus, it can be concluded that the EASM lifecycle has intensified, making it more likely for southwest Japan and Korea to experience heavy rainfall followed by enhanced drying. This result is in agreement with previous studies (Kim *et al* 2005, Seo *et al* 2013, In *et al* 2014) in terms of a generally intensified EASM system, but adds further details in that both the rainy season and dry spell within the EASM lifecycle have intensified. Apparently, the observed EASM variability is more complex than just the summer mean value.

The performance of CMIP6 models in simulating the EASM climatological evolution and its variability is still limited, but some models are showing sign of an improved performance. In general, the intensity of monsoon precipitation tends to be underestimated, but group A models realistically simulate the latitude-time propagation of the rainband and the general pattern of the long-term intensification of EASM. Not only that, group A models also depict the precipitation time-series at the active and break phase that is consistent with the observational dataset. While models in group B did not accurately simulate the progression of the summer rainband and they underestimated the EASM rainfall, they still depicted the rainfall peak in summer. This evaluation highlights some of CMIP6 models that exhibit a marked performance in simulating intraseasonal characteristic of the EASM as well as its long-term change.

Acknowledgments

This research is funded by the Korean Meteorological Agency under the grant KMI2018-07010 and GIST Research Institute (GRI) grant funded by the GIST in 2020. SYW is supported by US DOE Award No. DE-SC0016605 and SERDP Project No. RC-2709. HK acknowledges the Integrated Research Program for Advancing Climate Models (TOUGOU) JPMXD0717935457 from the MEXT and the Grant-in-Aid for Specially promoted Research 16H06291 from JSPS, Japan.

Data availability statement

The data that support the findings of the study are openly available. DOI for JRA-55 data is doi:10.5065/D6HH6H41, and ERA-interim is doi:10.5065/D6CR5RD9. The Unified CPC precipitation data is available at ftp://ftp.cdc.noaa.gov/Datasets/cpc_global_precip/, and CMIP6 is accessible at https://esgf-node.llnl.gov/search/cmip6/. OLR datasets is accessible at https://www.esrl.noaa.gov/psd/data/gridded/data.interp_OLR.html, GPCP dataset ftp://ftp.cgd.ucar.edu/archive/PRECIP/, and APHRODITE http://search.diasjp.net/en/dataset/APHRO_MA

ORCID iDs

Jina Park https://orcid.org/0000-0002-0439-8066
Hyungjun Kim https://orcid.org/0000-0003-1083-8416
S -Y Simon Wang https://orcid.org/0000-0003-2009-2275
Jee-Hoon Jeong https://orcid.org/0000-0002-3358-3949
Kyo-Sun Lim https://orcid.org/0000-0003-1468-9104
Matthew LaPlante https://orcid.org/0000-0001-6502-1492
Jin-Ho Yoon https://orcid.org/0000-0002-4939-8078

References

Barnes A A 1965 *Atmospheric Water Vapor Divergence: Measurements and Applications* (Ohio: Air Force Cambridge Research Laboratories, Office of Aerospace Research, United States Air Force)

Burke C and Stott P J J O C 2017 Impact of anthropogenic climate change on the East Asian summer monsoon *J. Clim.* **30** 5205–20

Chen T-C, Wang S-Y, Huang W-R and Yen M-C J J O-C 2004 Variation of the East Asian summer monsoon rainfall *J. Clim.* **17** 744–62

Dee D P et al 2011 The ERA-interim reanalysis: configuration and performance of the data assimilation system Q. J. R. Meteorol. Soc. 137 553–97
Ellis A W, Saffell E M and Hawkins T W 2004 A method for defining monsoon onset and demise in the southwestern USA J. R. Meteorol. Soc. 24 247–65
Harada Y, Kamahori H, Kobayashi C, Endo H, Kobayashi S, Ota Y, Onoda H, Onogi K, Miyaoka K and Takahashi K 2016 The JRA-55 reanalysis: representation of atmospheric circulation and climate variability J. Meteorol. Soc. Japan. Ser. II 94 269–302
Huffman G J, Adler R F, Morrissey M M, Bolvin D T, Curtis S, Joyce R, Mcgavock B and Susskind J 2001 Global precipitation at one-degree daily resolution from multisatellite observations J. Hydrometeorol. 2 36–50
Imada Y, Watanabe M, Kawase H, Shiogama H and Arai M J S 2019 The July 2018 high temperature event in Japan could not have happened without human-induced global warming SOLA 15A 8–12
In S-R, Han S-O, Im E-S, Kim K-H and Shim J J A 2014 Study on temporal and spatial characteristics of summertime precipitation over Korean Peninsula Atmosphere 24 159–71
Jin Y and Stan C J C C 2019 Changes of East Asian summer monsoon due to tropical air-sea interactions induced by a global warming scenario Clim. Change 153 341–59
Kim E-H, Kim M-K and Lee W-S 2005 The regional characteristics of daily precipitation intensity in Korea for recent 30 years J. Korean Earth Sci. Soc. 26 404–16
Knutti R, Furrer R, Tebaldi C, Cermak J and Meehl G A 2010 Challenges in combining projections from multiple climate models J. Clim. 23 2739–58
Kobayashi S et al 2015 The JRA-55 reanalysis: general specifications and basic characteristics J. Meteorol. Soc. Japan. Ser. II 93 5–48
Kornhuber K, Osprey S, Coumou D, Petri S, Petoukhov V, Rahmstorf S and Gray L 2019 Extreme weather events in early summer 2018 connected by a recurrent hemispheric wave-7 pattern Environ. Res. Lett. 14 054002
Li J, Wang B and Yang Y-M 2020 Diagnostic metrics for evaluating model simulations of the East Asian monsoon J. Clim. 33 1777–801
Li J, Wu Z, Jiang Z and He J 2010 Can global warming strengthen the East Asian summer monsoon? J. Clim. 23 6696–705
Liebmann B and Smith C A 1996 Description of a complete (interpolated) outgoing longwave radiation dataset Bull. Am. Meteorol. Soc. 77 1275–7
Liu J, Xu H and Deng J J E S D 2018 Projections of East Asian summer monsoon change at global warming of 1.5 and 2 °C Earth Syst. Dyn. 9 427–39
Madakumbura G D, Kim H, Utsumi N, Shiogama H, Fischer E M, Seland Ø, Scinocca J F, Mitchell D M, Hirabayashi Y and Oki T 2019 Event-to-event intensification of the hydrologic cycle from 1.5 °C to a 2 °C warmer world Sci. Rep. 9 3483
Park C et al 2020 Evaluation of summer precipitation over Far East Asia and South Korea simulated by multiple regional climate models Int. J. Climatol. 40 2270–84
Pradhan M, Rao A S, Srivastava A, Dakate A, Salunke K and Shameera K 2017 Prediction of Indian summer-monsoon onset variability: a season in advance Sci. Rep. 7 1–14
Seo K-H, Son J-H and Lee J-Y 2011 A new look at Changma Atmosphere 21 109–21
Seo K-H, Ok J, Son J-H and Cha D-H 2013 Assessing future changes in the East Asian summer monsoon using CMIP5 coupled models J. Clim. 26 7662–75
Singh D, Tsiang M, Rajaratnam B and Diffenbaugh N S 2014 Observed changes in extreme wet and dry spells during the South Asian summer monsoon season Nat. Clim. Change 4 456–61
Tallaksen L M, Madsen H and Clausen B 1997 On the definition and modelling of streamflow drought duration and deficit volume Hydrol. Sci. J. 42 15–33
Tian F, Dong B, Robson J, Sutton R and Tett S F 2019 Projected near term changes in the East Asian summer monsoon and its uncertainty Environ. Res. Lett. 14 084038
Tung Y-S, Wang S-Y S, Chu J-L, Wu C-H, Chen Y-M, Cheng C-T and Lin L-Y 2020 Projected increase of the East Asian summer monsoon (Meiyu) in Taiwan by climate models with variable performance Meteorol. Appl. 27 e1886
Utsumi N, Kim H, Kanae S and Oki T 2016 Which weather systems are projected to cause future changes in mean and extreme precipitation in CMIP5 simulations? J. Geophys. Res. Atmos. 121 10,522–537
Utsumi N, Kim H, Kanae S and Oki T 2017 Relative contributions of weather systems to mean and extreme global precipitation J. Geophys. Res. Atmos. 122 152–67
Wang S S Y, Kim H, Coumou D, Yoon J H, Zhao L and Gillies R R J A S L 2019 Consecutive extreme flooding and heat wave in Japan: are they becoming a norm? Atmos. Sci. Lett. 20 e933
Wang T, Miao J-P, Sun J-Q and Fu Y-H 2018 Intensified East Asian summer monsoon and associated precipitation mode shift under the 1.5 °C global warming target Adv. Clim. Change Res. 9 102–11
Woo S-H, Yim S-Y, Kwon M-H and Kim D-J 2017 Decadal change in rainfall during the changma period in early-2000s Atmosphere 27 345–58
Xie P, Yatagai A, Chen M, Hayasaka T, Fukushima Y, Liu C and Yang S 2007 A gauge-based analysis of daily precipitation over East Asia J. Hydrometeorol. 8 607–26
Yatagai A, Kamiguchi K, Arakawa O, Hamada A, Yasutomi N and Kitoh A 2012 APHRODITE: constructing a long-term daily gridded precipitation dataset for Asia based on a dense network of rain gauges Bull. Am. Meteorol. Soc. 93 1401–15
Yihui D and Chan J C 2005 The East Asian summer monsoon: an overview Meteorol. Atmos. Phys. 89 117–42
Yun K-S, Shin S-H, Ha K-J, Kitoh A and Kusunoki S 2008 East Asian precipitation change in the global warming climate simulated by a 20 km mesh AGCM Asia-Pac. J. Atmos. Sci. 44 233–47
Zhu C, Wang B, Qian W and Zhang B 2012 Recent weakening of northern East Asian summer monsoon: a possible response to global warming Geophys. Res. Lett. 39 L09701